Published in final edited form as:
Hepatology. 2012 April ; 55(4): 1215–1226. doi:10.1002/hep.24796.

Hepatocyte Growth Factor (HGF)/c-Met Signaling is required for Stem Cell Mediated Liver Regeneration

Tsuyoshi Ishikawa[*], **Valentina M. Factor**[*], **Jens U. Marquardt**, **Chiara Raggi**, **Daekwan Seo**, **Mitsuteru Kitade**, **Elizabeth A. Conner**, and **Snorri S. Thorgeirsson**[#]
Laboratory of Experimental Carcinogenesis, Center for Cancer Research, National Cancer Institute, NIH, Bethesda, United States

Abstract

HGF/c-Met supports a pleiotrophic signal transduction pathway that controls stem cell homeostasis. Here, we directly addressed the role of c-Met in stem cell-mediated liver regeneration by utilizing mice harboring *c-met* floxed alleles and Alb-Cre or Mx1-Cre transgenes. To activate oval cells, the hepatic stem cell (HSC) progeny, we used a model of liver injury induced by diet containing the porphyrinogenic agent, 3, 5-diethocarbonyl-1,4-dihydrocollidine (DDC). Deletion of *c-met* in oval cells was confirmed in both models by PCR analysis of FACS-sorted EpCam-positive cells. Loss of c-Met receptor decreased sphere-forming capacity of oval cells in vitro as well as reduced oval cell pool, impaired migration and decreased hepatocytic differentiation in vivo as demonstrated by double immunofluorescence using oval- (A6 and EpCam) and hepatocyte-specific (HNF-4α) antibodies. Furthermore, lack of c-Met had a profound effect on tissue remodeling and overall composition of HSC niche which was associated with greatly reduced MMP9 activity and decreased expression of SDF1. Using a combination of double immunofluorescence of cell type-specific markers with MMP9 and gelatin zymography on the isolated cell populations, we identified macrophages as a major source of MMP9 in DDC-treated livers. The Mx1-Cre-driven *c-met* deletion caused the greatest phenotypic impact on HSCs response as compared to the selective inactivation in the epithelial cell lineages achieved in c-Met$^{fl/fl}$; Alb-Cre$^{+/-}$ mice. However, in both models, genetic loss of *c-met* triggered a similar cascade of events leading to failure of HSCs mobilization and death of the mice. Conclusion: These results establish a direct contribution of c-Met in regulation of HSC response, and support a unique role for HGF/c-Met as an essential growth factor signaling pathway for regeneration of diseased liver.

Keywords

Oval cell; DDC model; MMP9; hepatic stem cell niche; Kupffer cell

It is now well recognized that adult liver contains a stem cell compartment that can be activated under conditions of severe liver injury to give rise to both hepatocytic and biliary epithelial cell (BEC) lineages[1-4]. Hepatic stem cells (HSC) are thought to reside within the terminal bile ductules (Hering Canals) located at the interface between parenchyma and biliary tracts. Upon activation, HSC give rise to oval cells which form a network of proliferating brunching ducts that migrate into parenchyma where they finally differentiate into hepatocytes[5-7]. Numerous molecular factors and cell types contribute to HSC activation either directly or indirectly[8-10]. We and others have established that oval cell expansion

[#]Address requests for reprints to: Snorri S. Thorgeirsson, MD, PhD, National Cancer Institute, Building 37, Room 4146A, 37 Convent Drive, Bethesda, Maryland 20892-4262. Snorri_thorgeirsson@nih.gov; fax: (301) 496-0734.
[*]Both authors contributed equally to the work

requires a close cooperation with accompanying stellate cells which provides hepatocyte growth factor (HGF) and also promote pericellular collagen deposition thus creating a microenvironment supporting growth of expanding progenitor cells[11-16].

HGF was originally characterized as a potent mitogen for mature hepatocytes[17]. All biological effects of HGF are mediated by a single tyrosine kinase receptor c-Met[18-19]. Gene knockout studies have shown that both HGF and c-Met are absolutely required for survival including liver development[20-21]. The unique property of c-Met signaling is activation of a complex biological program supporting morphogenesis, mitogenesis and motogenesis (also referred to as ”invasive growth”)[22-23].The program operates during embryogenesis, tissue regeneration and cancer metastasis, and controls proliferation, branching morphogenesis, survival, migration through ECM, and differentiation. Previously, we have shown that HGF/c-Met signaling promotes activation and early expansion of oval cells following severe liver injury in an AAF+PH rat model[12]. However, the molecular mechanisms supporting adult stem cell activation are not well understood, and knowledge about the role of HGF/c-Met pathway in this process is still limited.

Recently, we and others have provided direct genetic evidence for the essential role of HGF/c-Met in hepatocyte-mediated liver regeneration[24-26]. Here, we analyzed the contribution of the c-Met signaling pathway in stem cell-mediated liver regeneration by utilizing liver-specific c-Met conditional knockout mice. To gain insight in the intricate nature of epithelial-mesenchymal cross-talk that defines the stem cell behavior, inactivation of c-Met was achieved either in epithelial cell lineages (c-Met$^{fl/fl}$; Alb-Cre$^{+/-}$) or in various subsets of liver cells including stromal cells (c-Met$^{fl/fl}$; Mx1-Cre$^{+/-}$) by crossing c- Met$^{fl/fl}$ mice with transgenic mice expressing Cre-recombinase under the control of constitutively active albumin promoter or ubiquitous interferon-inducible Mx1 promoter. To activate oval cells, we used a model of chronic liver injury induced by diet containing the porphyrinogenic agent, 3, 5-diethocarbonyl-1,4-dihydrocollidine (DDC), which have been described previously[27-28].

Our results show that the absence of c-Met caused severe damage both to hepatocytes and biliary epithelium, disrupted the balance between extracellular matrix production and degradation and prevented stem cell-mediated liver regeneration. Consequently, our study establishes the HGF/c-Met signaling pathway as an essential component of the hepatic regenerative capability.

Materials and Methods

Mice and treatments

Male 8-10 week old Met$^{fl/fl}$;Mx1-Cre$^{+/-}$ and c-Met$^{fl/fl}$; Alb-Cre$^{+/-}$ mice were generated and genotyped as described[25-26]. Met$^{fl/fl}$ and c-Met$^{wt/wt}$; Alb-Cre$^{+/-}$ mice were used as corresponding controls. For Mx1-Cre mediated c-Met inactivation, Met$^{fl/fl}$ and Met$^{fl/fl}$; Mx1-Cre$^{+/-}$ mice received three i.p. injections of 300 μg of pIpC in saline at 2-day intervals which in liver was shown to result in a complete deletion of gene flanked by LoxP recombinase recognition sites[29]. To induce oval cells, mice were given a diet containing 0.1% DDC (Bioserv, Frenchtown, NJ). Met$^{fl/fl}$; Mx1-Cre$^{+/-}$ and Met$^{fl/fl}$ mice received DDC diet 3days after the last pIpC injection. Mice were housed in an AAALAC facility and cared for in accordance with the guidelines from the Animal Care and Use Committee at the National Cancer Institute, NIH.

Gelatin and in situ zymography

The activity of MMPs in tissue extracts was examined by electrophoresis on 10% sodium dodecyl sulfate polymerase acrylamide gel electrophoresis (SDS-PAGE) containing gelatin

(Invitrogen, CA) without prior heating or reduction. Gels were stained with SimplyBlue SafeStain (Invitrogen, CA). Densitometry was performed on inverted black and white gel images. In situ zymography was performed on 7 μm liver cryosections as described[30].

Statistical Analysis

The statistical differences for two-group comparison were determined by Bootstrap-t-test with 10,000 repetitions for small sample sizes ($n < 4$), and by two samples Student's t-test or Mann–Whitney U-test for a larger sample size. Kolmogorov-Smirnov test and Leven's test were used to verify the normality assumption and equality of variances, respectively. For three-group comparison, one-way ANOVA test was applied if the samples satisfied normality assumption, and Kruskal-Wallis rank sum test, if the samples failed normality assumption. For a discrete random variable, the statistical differences were determined using Poisson generalized linear model. We used the R statistical software (v. 2.8.0) and considered *P* values ≤ 0.05 (*), ≤ 0.01 (**), and ≤ 0.001 (***) as significant.

Results

Lack of c-Met induces severe liver dysfunction, fibrosis, and cholestasis

The phenotype of both c-Met mutant mice was very similar albeit more severe in mice with total (c-Met$^{fl/fl}$; Mx1-Cre$^{+/-}$) rather than selective (c-Met$^{fl/fl}$; Alb-Cre$^{+/-}$) c-Met inactivation (Fig. 1, Supporting Fig. 1). In both cases, Met-deficient mice did not show compensatory regeneration and developed severe liver atrophy due to significant reduction in hepatocyte proliferation and parallel increase in hepatocyte apoptosis (Fig.1A-C; Supporting Fig.1A-C). Consistent with more extensive liver damage, both conditional knockout models displayed considerable decrease in serum albumin levels (Fig.1D; Supporting Fig. 1D) while the levels of aspartate aminotransferase, alkaline phosphatase and direct bilirubin were progressively increasing (Fig.1E; Supporting Fig. 1E-I).

At the molecular level, c-Met mutant livers were unable to activate the major downstream signaling pathways involved in cell proliferation, motility regulation and apoptosis protection, such as extracellular signal-regulated kinases (Erk1/2), Akt, and Stat3 (Fig. 1F). Histologically, the most striking difference was a considerable reduction in oval cell proliferation. Control livers developed an extensive network of branching oval cell ducts with small lumens radiating from the periportal areas toward the parenchyma. In contrast, the mutant epithelium displayed a dramatic accumulation of protoporphyrin plugs and showed only a rudimentary outgrowth which was more reminiscent of a classical bile duct proliferation restricted by a more severe periportal fibrosis (Supporting Fig. 2). By 8 week of DDC treatment, all c-Met$^{fl/fl}$; Mx1-Cre$^{+/-}$ and c-Met$^{fl/fl}$; Alb-Cre$^{+/-}$ mice (n=5 each genotype) died from liver failure whereas all control mice survived (n=10). Together the data show that the absence of c-Met function caused severe damage to both hepatocytes and biliary epithelium, impaired oval cell expansion, and thus blocked liver regeneration.

Lack of c-Met affects sphere-forming capacity of oval cells

Sphere-forming assays are widely used in stem cell biology to determine the dynamics of stem cells in vivo[31]. To address the sphere-forming potential of c-Met deleted oval cells, we first isolated the bulk nonparenchymal cell fraction and FACS-sorted single oval cells using an oval cell-specific marker EpCam[32] in combination with lineage cocktail antibodies. The latter are designed to react with five major hematopoietic lineages and were used to ensure the purity of the FACS-sorted epithelial cells. We confirmed that *c-met* was deleted in the EpCam^{+}/Lineage^{-} cells in both models, as shown by PCR analysis (Fig. 2A,B).

To generate spheres, we then cultured the sorted EpCam^{+}/Lineage^{-} cells in matrigel in the presence of HGF, EGF, or both growth factors. Quantification and morphological assessment of cultures showed that the number of primary spheres generated from the c-Met deleted oval cells was reduced by 80%. In addition, the mutant spheres were considerably smaller (Fig. 2C,D). As expected, c-Met deficient cells were responsive only to mitogenic EGF but not HGF. In c-Met expressing cells, HGF alone was more effective in increasing both the number and the sphere size as compared to EGF. These experiments demonstrate that *c-met* deletion altered functional properties of oval cells.

Lack of c-Met affects oval cell proliferation

To corroborate these findings in vivo, we used Ki-67 immunohistochemistry. A quantitative time course analysis of Ki-67-staining showed a drastic and progressive decline in the frequency of proliferating oval in c-Met deficient livers (Fig.3A). Reduction in proliferation was found in both c-Met models as shown by a similar decrease in the oval cell density as determined by the quantification of the number of A6-positive cells (Fig. 3B). Immunostaining with additional marker of cell cycle progression confirmed a significant decrease in the size of oval cell pool (Fig.3C). Interestingly, loss of Met appeared to be more compatible with BEC proliferation (Fig. 3C, bottom images) implying a failure of oval cell outgrowth.

Lack of c-Met affects oval cell differentiation

To test whether the differentiation potency of oval cells was impaired, we performed dual-label experiments using two oval cell specific antibodies, A6 and EpCam. Our previous work has established that A6 in addition to being a specific marker of oval cells and BEC, can also recognize a fraction of newly formed hepatocytes[33-34] while EpCam is expressed exclusively by oval and bile duct cells[32, 35]. Quantitative analysis revealed a progressive accumulation of A6^{+}/EpCam^{-} positive cell clusters with a hepatocyte-like morphology which were located in close vicinity to oval cells only in the Met$^{fl/fl}$ control livers but not in c-Met$^{fl/fl}$; Mx1-Cre$^{+/-}$ or c-Met$^{fl/fl}$; Alb-Cre$^{+/-}$ livers (Fig. 4A,B; and not shown). Significantly, only A6^{+} hepatocyte-like cells expressed HNF4α transcription factor, a well known marker of hepatocytic differentiation[36] whereas ductular oval cells were HNF4α-negative (Fig. 4C). These data demonstrate that loss of c-Met impaired the ability of oval cells to differentiate into hepatocytic lineage.

Lack of c-Met affects oval cell migration

Next, we examined the changes in distribution of oval cells migrating inside the parenchyma. For this, we divided the hepatic lobule into three zones, periportal (0-97 μm), middle (97-194 μm), and central (194-290 μm), and measured the distance between the portal tract and migrating oval cells visualized by A6 staining. In control livers, oval cells formed small ducts expanding toward central zone (Fig. 5). The average distance between the portal veins and end point of A6-positive small brunching ducts with poorly defined lumen increased from 92.6 μm at 1 week to 132.7 μm at 4 weeks. In contrast, in c-Met-deficient livers, A6-positive cells lined larger ducts with round lumen which were confined to portal tracts and did not spread into parenchyma (the average distance from portal tract 78.2 μm and 79.0 μm at 1 and 4 weeks, respectively) (Fig. 5A-C). Thus, the absence of c-Met altered the pattern of ductular reaction and impaired its distribution in the parenchyma.

Loss of c-Met in HSCs alters functional interactions with stem cell niche microenvironment

Next, we assessed whether the absence of c-Met signaling altered stem cell/oval cell micro-environment. Consistent with the protective role of HGF/c-Met against fibrosis[37], both c-

Met mutant models developed a more extensive periportal fibrosis as judged by quantification of Sirius red staining which was more pronounced in c-Met$^{fl/fl}$; Mx1-Cre$^{+/-}$ livers (Fig. 6A-B). By 4 weeks after initiation of DDC diet, the Sirius red-positive areas were significantly larger both in c-Met$^{fl/fl}$; Mx1-Cre$^{+/-}$ and in c-Met$^{fl/fl}$; Alb-Cre$^{+/-}$ livers as compared to the respective DDC-treated control mice (Fig. 6C). Monitoring liver fibrosis using second harmonic generation confocal imaging confirmed the presence of much more dense and altered collagen matrix structure in c-Met deficient mice maintained on DDC diet (Fig.6A). In contrast with straight and well organized collagen fibers in DDC-treated control livers, mutant livers displayed irregular, wavy, and significantly less aligned collagen fibers or bundles.

This was paralleled by a diminished macrophage mobilization as measured by immunohistochemistry and FACS analysis using Kupffer cell-specific F4/80 antibody (Fig. 6A, E,F). Remarkably, both total and selective c-Met inactivation in liver cells decreased recruitment of stromal/inflammatory cells to the site of oval cell reaction suggesting a leading role for epithelial compartment in maintaining functional HSC microenvironment.

Decreased fibrolytic activity in c-Met deficient mice

To address the mechanisms underlying increased fibrosis and aberrant tissue remodeling in c-Met deleted livers, we examined the levels of MMPs, the primary proteolytic enzymes involved in the breakdown of ECM. A time course of MMP9 activation showed that in control mice, the proteolytic activity of the MMP9 was progressively increasing along with the expansion of oval cells whereas c-Met deficient mice displayed a decrease in MMP9 (Fig. 7A,B). This was consistent with the results of in situ zymography combined with A6 staining which showed a close proximity of MMP9 activity to oval cell reaction (Fig. 7C; Supporting Fig.3). The levels of MMP9 were reduced in both models of liver-specific and epithelial specific c-Met deletion (Fig. 7D,E). There was no difference in MMP2 activity regardless of genotype. These data link the aberrant tissue remodeling in c-Met deficient livers with reduction in stem cell niche component MMP9.

Cell source of MMP9

Finally, we determined the cell source of MMP9 in DDC-treated livers. For this, we carried out gelatin zymography on isolated hepatocytes, nonparenchymal cell (NPC) fraction and FACS-sorted F4/80-positive macrophages. Quantification of the intensity of active MMP9 band showed that the main source of active MMP9 was NPC cells, and that monocytes/macrophages accounted for about 80% of this activity (Fig. 8A,B). Confirming the zymography results, dual immunofluorescence staining for MMP9 and markers for oval (A6), Kupffer (F4/80), and stellate (αSMA) cells revealed the co-localization at the interface with Kupffer and oval cells, but not with stellate cells (Fig. 8C). These data show that macrophage is the primary cell source of active MMP9 in this model. To provide additional evidence that absence of c-Met creates a defective stem cell microenvironment, we examined the expression of chemokine stromal derived factor (SDF1), known as a powerful chemo-attractant for the bone marrow derived monocytes. The SDF1 protein levels were considerably decreased in both Met mutant models as well as the number of A6^{+}/SDF1^{+} oval cells (Supporting Fig. 4).

Discussion

The goal of this study was to define the role of c-Met signaling pathway in different phases of adult hepatic stem cell activation by utilizing mice harboring *c-met* floxed alleles and Alb-Cre or Mx1-Cre transgenes. Using conditional mouse genetics and DDC toxic liver injury model, we demonstrate that lack of c-Met signals impaired both hepatocyte and stem

cell-mediated liver regeneration, leading to the death of mice. Genetic loss of c-Met function has profound effects on tissue remodeling and overall composition of the hepatic stem cell niche microenvironment concomitant with a failure of hepatic stem cells to expand and to differentiate into hepatocytes. The Mx1-Cre-driven deletion of *c-met* in liver cells resulted in a more severe impact on stem cell activation as compared to the selective inactivation of *c-met* in the epithelial cell lineages achieved in c-Met$^{fl/fl}$; Alb-Cre$^{+/-}$ mice. However, in both models, loss of c-Met function caused a similar cascade of events disrupting HSC response.

Consistent with the c-Met involvement in diverse cellular functions, *c-met* deletion had a broad and profound impact on hepatic stem cell properties. Assessment of proliferation and the frequency of oval cells, hepatic stem cell progeny, using a combination of oval cell specific and proliferative markers revealed a striking decrease in the size of oval cell pool (Fig.3). We also found a marked reduction in the number of A6^{+}/HNF4α^{+} cells, reflecting a reduced capacity of c-Met deficient oval cells to differentiate into hepatocytes (Fig. 4) as well as almost complete lack of their migration into parenchyma (Fig. 5).

Concurring with fewer oval cells being present in c-Met mutant livers, the frequency of primary spheres generated from EpCam^{+}/Lineage^{-} cells isolated from both c-Met$^{fl/fl}$; Mx1-Cre$^{+/-}$ and c-Met$^{fl/fl}$; Alb-Cre$^{+/-}$ mutant livers was significantly reduced as compared to the sphere forming activity of c-Met expressing oval cells (Fig.2). The c-Met deficient spheres were smaller in size and failed to attach and expand in 2D monolayer while control spheres could be further sub-cultured as adherent clones. These data provide a strong indication that c-Met signals play a prominent role not only in hepatocyte proliferation[24-26] but also impact the dynamics of hepatic progenitor cells in vivo. Significantly, EGF supplementation was capable to increase the sphere-forming ability of c-Met deficient oval cells to the levels found in the similarly treated control cells. These in vitro experiments suggest that signaling molecules shared by tyrosine kinase receptors could compensate at least in part for the lack of c-Met. This was in striking contrast to the situation in vivo where hepatic deletion of a single *c-met* gene caused far-reaching alterations in hepatic homeostasis and created a microenvironment which compromised normal stem cell functions via direct and indirect mechanisms.

Significantly, c-Met deficiency promoted development of the periportal fibrosis consistent with the antifibrotic role of HGF/c-Met signaling[37]. High-resolution imaging of primary fibrillar collagens in unfixed livers using second-harmonic generation microscopy[38] corroborated a denser collagen distribution and also revealed prominent differences in the orientation and length of collagen fibers. Furthermore, c-Met deficiency caused an aberrant tissue distribution of the collagen producing stellate cells (Fig.6). In contrast with control livers, in both models of c-Met deletion, stellate cells did not accompany the migrating oval cells but accumulated in the areas of periportal fibrosis. Our previous results as well as others implicated hepatic stellate cells as an integral component of hepatic stem cell niche by providing a variety of growth factors as well as a mechanical support for expanding population of oval cells[11-16].

Another striking consequence of c-Met deficiency was defective mobilization of F4/80-positive Kupffer cells and greatly reduced secretion of proteolytic enzyme MMP9 at the margins of adjacent oval cells disrupting the balance between extracellular matrix production and degradation (Fig. 7, Supporting Fig. 3). The structural abnormalities caused by the lack of c-Met function could compromise the movement of the expanding oval cell ducts into parenchyma and thereby interrupt cross-talks with the components of hepatic stem cell niche. This phenomenon occurred regardless of total or selective c-Met inactivation in liver cells although it was more prominent in Met$^{fl/fl}$; Mx1-Cre$^{+/-}$ mice, suggesting that loss

of c-Met function in the epithelial compartment was a common denominator responsible for the striking similarities in phenotypes.

MMP9 is a matrix degrading enzyme involved in the resolution of fibrotic matrix and basement membrane degradation[39] critical for oval cell migration into parenchyma and subsequent differentiation into hepatocytes[6, 40-41]. Using a combination of double immunofluorescence of MMP9 with cell type specific markers as well as gelatin zymography on the isolated cell populations, we identified macrophages as a major source of MMP9 in DDC-treated livers (Fig.8). These data are in line with the early reports describing macrophages as the primary source of gelatinases in liver fibrosis[42]. The invading macrophages have been also referred to as major determinants of liver progenitor cell expansion in the models of diet- and immune-mediated liver injury by providing promitogenic cytokines (e.g. TNFα, TWEAK)[15, 43-45] and MMPs, including MMP9[46].

In addition to matrix degrading potential, MMP9 is also known for its ability to recruit bone marrow-derived cells to injured liver to facilitate resolution of fibrotic matrix[47-48]. As a part of a general impairment of tissue remodeling caused by the c-Met absence, we also found reduced levels of SDF-1 (Supplemental Fig.4), another stem cell niche mediator which can attract and retain hematopoietic cells within fibrotic livers[47].

Cre-mediated recombination of $Met^{fl/fl}$ was achieved both in hepatocytes and ductular oval/biliary epithelial cells regardless of using Mx1-Cre or Alb-Cre promoter, similar to the findings published previously[49-50]. Accordingly, these two epithelial cell types sustained a considerable structural and functional damage as shown by reduced albumin secretion and a marked increase in serum aspartate aminotransferase levels (Fig. 1; Supporting Fig. 1). Consistent with a protective role of HGF/c-Met signaling against accumulating toxic bile acids and developing intrahepatic cholesterol[51], both c-Met conditional knockout mouse models also displayed a marked increase in serum bile acid and bilirubin concentrations rendering c-Met mice more susceptible to DDC toxic injury. Thus, the combined impact of increased bile acid production and a defective hepatobiliary transport capacity appear to contribute to increased cholestasis and liver injury promoted by the lack of c-Met signaling. The latter underscores the fundamental role of HGF/c-Met signaling pathway for regeneration of diseased liver.

In summary, using a DDC toxic liver injury model we have showed that c-Met is a major determinant of adult hepatic stem cell and HSC niche homeostasis. Lack of c-Met affected proliferative potential of oval cells, capacity to migrate, pattern of differentiation and dynamic interaction with microenvironment. Future studies aiming at isolating and characterizing oval cells induced by other models of liver injury relevant to human studies (e.g. viral injury, acetaminophen toxicity, bile duct ligation) will further understanding of the role of c-Met signaling in regulation of adult liver stem cells.

Supplementary Material

Refer to Web version on PubMed Central for supplementary material.

Acknowledgments

We thank Dr. Joe Grisham for valuable discussions; Susan Garfield for the help with confocal microscopy, and Tanya Hoang and Anita Ton for their assistance with PCR analysis, immunohistochemistry and animal care.

Financial Support: This research was supported by the Intramural Research Program of the NIH, National Cancer Institute.

References

1. Evarts RP, Nagy P, Marsden E, Thorgeirsson SS. A precursor-product relationship exists between oval cells and hepatocytes in rat liver. Carcinogenesis. 1987; 8:1737–1740. [PubMed: 3664968]
2. Thorgeirsson SS, Evarts RP, Bisgaard HC, Fujio K, Hu Z. Hepatic stem cell compartment: activation and lineage commitment. Proc Soc Exp Biol Med. 1993; 204:253–260. [PubMed: 7694304]
3. Thorgeirsson SS, Grisham JW. Overview of recent experimental studies on liver stem cells. Semin Liver Dis. 2003; 23:303–312. [PubMed: 14722808]
4. Duncan AW, Dorrell C, Grompe M. Stem cells and liver regeneration. Gastroenterology. 2009; 137:466–481. [PubMed: 19470389]
5. Theise ND, Saxena R, Portmann BC, Thung SN, Yee H, Chiriboga L, Kumar A, et al. The canals of Hering and hepatic stem cells in humans. Hepatology. 1999; 30:1425–1433. [PubMed: 10573521]
6. Paku S, Schnur J, Nagy P, Thorgeirsson SS. Origin and structural evolution of the early proliferating oval cells in rat liver. Am J Pathol. 2001; 158:1313–1323. [PubMed: 11290549]
7. Riehle KJ, Dan YY, Campbell JS, Fausto N. New concepts in liver regeneration. J Gastroenterol Hepatol. 2011; 26(Suppl 1):203–212. [PubMed: 21199532]
8. Roskams T, Katoonizadeh A, Komuta M. Hepatic progenitor cells: an update. Clin Liver Dis. 2010; 14:705–718. [PubMed: 21055691]
9. Greenbaum LE, Wells RG. The role of stem cells in liver repair and fibrosis. Int J Biochem Cell Biol. 2011; 43:222–229. [PubMed: 19914396]
10. Tanaka M, Itoh T, Tanimizu N, Miyajima A. Liver stem/progenitor cells: their characteristics and regulatory mechanisms. J Biochem. 2011; 149:231–239. [PubMed: 21217146]
11. Evarts RP, Hu Z, Fujio K, Marsden ER, Thorgeirsson SS. Activation of hepatic stem cell compartment in the rat: role of transforming growth factor alpha, hepatocyte growth factor, and acidic fibroblast growth factor in early proliferation. Cell Growth Differ. 1993; 4:555–561. [PubMed: 7691152]
12. Hu Z, Evarts RP, Fujio K, Marsden ER, Thorgeirsson SS. Expression of hepatocyte growth factor and c-met genes during hepatic differentiation and liver development in the rat. Am J Pathol. 1993; 142:1823–1830. [PubMed: 8506951]
13. Sawitza I, Kordes C, Reister S, Haussinger D. The niche of stellate cells within rat liver. Hepatology. 2009; 50:1617–1624. [PubMed: 19725107]
14. Van Hul NK, Abarca-Quinones J, Sempoux C, Horsmans Y, Leclercq IA. Relation between liver progenitor cell expansion and extracellular matrix deposition in a CDE-induced murine model of chronic liver injury. Hepatology. 2009; 49:1625–1635. [PubMed: 19296469]
15. Lorenzini S, Bird TG, Boulter L, Bellamy C, Samuel K, Aucott R, Clayton E, et al. Characterisation of a stereotypical cellular and extracellular adult liver progenitor cell niche in rodents and diseased human liver. Gut. 2010; 59:645–654. [PubMed: 20427399]
16. Pintilie DG, Shupe TD, Oh SH, Salganik SV, Darwiche H, Petersen BE. Hepatic stellate cells' involvement in progenitor-mediated liver regeneration. Lab Invest. 2010; 90:1199–1208. [PubMed: 20440274]
17. Michalopoulos GK, DeFrances MC. Liver regeneration. Science. 1997; 276:60–66. [PubMed: 9082986]
18. Nakamura T, Mizuno S. The discovery of hepatocyte growth factor (HGF) and its significance for cell biology, life sciences and clinical medicine. Proc Jpn Acad Ser B Phys Biol Sci. 2010; 86:588–610.
19. Trusolino L, Bertotti A, Comoglio PM. MET signalling: principles and functions in development, organ regeneration and cancer. Nat Rev Mol Cell Biol. 2010; 11:834–848. [PubMed: 21102609]
20. Schmidt C, Bladt F, Goedecke S, Brinkmann V, Zschiesche W, Sharpe M, Gherardi E, et al. Scatter factor/hepatocyte growth factor is essential for liver development. Nature. 1995; 373:699–702. [PubMed: 7854452]
21. Uehara Y, Minowa O, Mori C, Shiota K, Kuno J, Noda T, Kitamura N. Placental defect and embryonic lethality in mice lacking hepatocyte growth factor/scatter factor. Nature. 1995; 373:702–705. [PubMed: 7854453]

22. Gao CF, Vande Woude GF. HGF/SF-Met signaling in tumor progression. Cell Res. 2005; 15:49–51. [PubMed: 15686627]
23. Gentile A, Trusolino L, Comoglio PM. The Met tyrosine kinase receptor in development and cancer. Cancer Metastasis Rev. 2008; 27:85–94. [PubMed: 18175071]
24. Borowiak M, Garratt AN, Wustefeld T, Strehle M, Trautwein C, Birchmeier C. Met provides essential signals for liver regeneration. Proc Natl Acad Sci U S A. 2004; 101:10608–10613. [PubMed: 15249655]
25. Huh CG, Factor VM, Sanchez A, Uchida K, Conner EA, Thorgeirsson SS. Hepatocyte growth factor/c-met signaling pathway is required for efficient liver regeneration and repair. Proc Natl Acad Sci U S A. 2004; 101:4477–4482. [PubMed: 15070743]
26. Factor VM, Seo D, Ishikawa T, Kaposi-Novak P, Marquardt JU, Andersen JB, Conner EA, et al. Loss of c-Met disrupts gene expression program required for G2/M progression during liver regeneration in mice. PLoS One. 2010; 5
27. Preisegger KH, Factor VM, Fuchsbichler A, Stumptner C, Denk H, Thorgeirsson SS. Atypical ductular proliferation and its inhibition by transforming growth factor beta1 in the 3,5-diethoxycarbonyl-1,4-dihydrocollidine mouse model for chronic alcoholic liver disease. Lab Invest. 1999; 79:103–109. [PubMed: 10068199]
28. Wang X, Willenbring H, Akkari Y, Torimaru Y, Foster M, Al-Dhalimy M, Lagasse E, et al. Cell fusion is the principal source of bone-marrow-derived hepatocytes. Nature. 2003; 422:897–901. [PubMed: 12665832]
29. Kuhn R, Schwenk F, Aguet M, Rajewsky K. Inducible gene targeting in mice. Science. 1995; 269:1427–1429. [PubMed: 7660125]
30. Masson V, de la Ballina LR, Munaut C, Wielockx B, Jost M, Maillard C, Blacher S, et al. Contribution of host MMP-2 and MMP-9 to promote tumor vascularization and invasion of malignant keratinocytes. FASEB J. 2005; 19:234–236. [PubMed: 15550552]
31. Pastrana E, Silva-Vargas V, Doetsch F. Eyes wide open: a critical review of sphere-formation as an assay for stem cells. Cell Stem Cell. 2011; 8:486–498. [PubMed: 21549325]
32. Okabe M, Tsukahara Y, Tanaka M, Suzuki K, Saito S, Kamiya Y, Tsujimura T, et al. Potential hepatic stem cells reside in EpCAM+ cells of normal and injured mouse liver. Development. 2009; 136:1951–1960. [PubMed: 19429791]
33. Engelhardt NV, Factor VM, Yasova AK, Poltoranina VS, Baranov VN, Lasareva MN. Common antigens of mouse oval and biliary epithelial cells. Expression on newly formed hepatocytes Differentiation. 1990; 45:29–37.
34. Factor VM, Radaeva SA, Thorgeirsson SS. Origin and fate of oval cells in dipin-induced hepatocarcinogenesis in the mouse. Am J Pathol. 1994; 145:409–422. [PubMed: 8053498]
35. Tanaka M, Okabe M, Suzuki K, Kamiya Y, Tsukahara Y, Saito S, Miyajima A. Mouse hepatoblasts at distinct developmental stages are characterized by expression of EpCAM and DLK1: drastic change of EpCAM expression during liver development. Mech Dev. 2009; 126:665–676. [PubMed: 19527784]
36. Parviz F, Matullo C, Garrison WD, Savatski L, Adamson JW, Ning G, Kaestner KH, et al. Hepatocyte nuclear factor 4alpha controls the development of a hepatic epithelium and liver morphogenesis. Nat Genet. 2003; 34:292–296. [PubMed: 12808453]
37. Giebeler A, Boekschoten MV, Klein C, Borowiak M, Birchmeier C, Gassler N, Wasmuth HE, et al. c-Met confers protection against chronic liver tissue damage and fibrosis progression after bile duct ligation in mice. Gastroenterology. 2009; 137:297–308. 308 e291-294. [PubMed: 19208365]
38. Zipfel WR, Williams RM, Christie R, Nikitin AY, Hyman BT, Webb WW. Live tissue intrinsic emission microscopy using multiphoton-excited native fluorescence and second harmonic generation. Proc Natl Acad Sci U S A. 2003; 100:7075–7080. [PubMed: 12756303]
39. Bellayr IH, Mu X, Li Y. Biochemical insights into the role of matrix metalloproteinases in regeneration: challenges and recent developments. Future Med Chem. 2009; 1:1095–1111. [PubMed: 20161478]
40. Paku S, Nagy P, Kopper L, Thorgeirsson SS. 2-acetylaminofluorene dose-dependent differentiation of rat oval cells into hepatocytes: confocal and electron microscopic studies. Hepatology. 2004; 39:1353–1361. [PubMed: 15122764]

41. Pham Van T, Couchie D, Martin-Garcia N, Laperche Y, Zafrani ES, Mavier P. Expression of matrix metalloproteinase-2 and -9 and of tissue inhibitor of matrix metalloproteinase-1 in liver regeneration from oval cells in rat. Matrix Biol. 2008; 27:674–681. [PubMed: 18678246]
42. Fallowfield JA, Mizuno M, Kendall TJ, Constandinou CM, Benyon RC, Duffield JS, Iredale JP. Scar-associated macrophages are a major source of hepatic matrix metalloproteinase-13 and facilitate the resolution of murine hepatic fibrosis. J Immunol. 2007; 178:5288–5295. [PubMed: 17404313]
43. Jakubowski A, Ambrose C, Parr M, Lincecum JM, Wang MZ, Zheng TS, Browning B, et al. TWEAK induces liver progenitor cell proliferation. J Clin Invest. 2005; 115:2330–2340. [PubMed: 16110324]
44. Tirnitz-Parker JE, Viebahn CS, Jakubowski A, Klopcic BR, Olynyk JK, Yeoh GC, Knight B. Tumor necrosis factor-like weak inducer of apoptosis is a mitogen for liver progenitor cells. Hepatology. 2010; 52:291–302. [PubMed: 20578156]
45. Viebahn CS, Benseler V, Holz LE, Elsegood CL, Vo M, Bertolino P, Ganss R, et al. Invading macrophages play a major role in the liver progenitor cell response to chronic liver injury. J Hepatol. 2010; 53:500–507. [PubMed: 20561705]
46. Kallis YN, Robson AJ, Fallowfield JA, Thomas HC, Alison MR, Wright NA, Goldin RD, et al. Remodelling of extracellular matrix is a requirement for the hepatic progenitor cell response. Gut. 2011; 60:525–533. [PubMed: 21106552]
47. Kollet O, Shivtiel S, Chen YQ, Suriawinata J, Thung SN, Dabeva MD, Kahn J, et al. HGF, SDF-1, and MMP-9 are involved in stress-induced human CD34+ stem cell recruitment to the liver. J Clin Invest. 2003; 112:160–169. [PubMed: 12865405]
48. Higashiyama R, Inagaki Y, Hong YY, Kushida M, Nakao S, Niioka M, Watanabe T, et al. Bone marrow-derived cells express matrix metalloproteinases and contribute to regression of liver fibrosis in mice. Hepatology. 2007; 45:213–222. [PubMed: 17187438]
49. Apte U, Thompson MD, Cui S, Liu B, Cieply B, Monga SP. Wnt/beta-catenin signaling mediates oval cell response in rodents. Hepatology. 2008; 47:288–295. [PubMed: 17929301]
50. van Hengel J, D'Hooge P, Hooghe B, Wu X, Libbrecht L, De Vos R, Quondamatteo F, et al. Continuous cell injury promotes hepatic tumorigenesis in cdc42-deficient mouse liver. Gastroenterology. 2008; 134:781–792. [PubMed: 18325391]
51. Song KH, Ellis E, Strom S, Chiang JY. Hepatocyte growth factor signaling pathway inhibits cholesterol 7alpha-hydroxylase and bile acid synthesis in human hepatocytes. Hepatology. 2007; 46:1993–2002. [PubMed: 17924446]

Abbreviations

DDC	a 3,5-diethoxycarbonyl-1,4-dihydro-collidin
BEC	biliary epithelial cell
PV	portal vein
CV	central vein
NPC	non-parenchymal cell

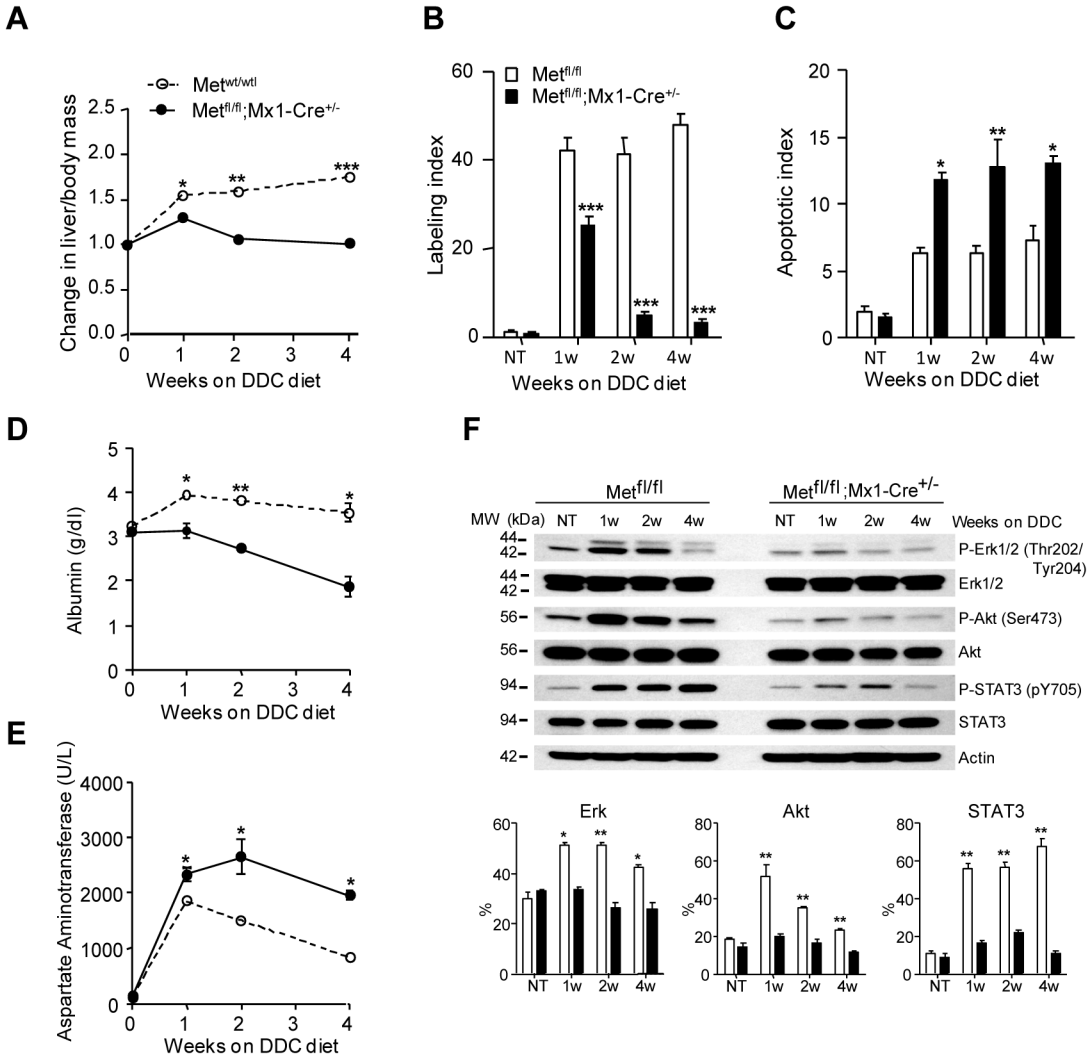

Fig. 1.

Genetic deletion of c-Met blocks liver regeneration and impairs liver function in DDC-treated mice. (A) Time course changes in liver-to-body mass ratio during DDC treatment shown as means ± SEM (n=5). (B, C) Reduced DNA replication and increased apoptosis. The number of Ki-67-positive (labeling index) and TUNEL-positive hepatocytes (apoptotic index) was evaluated in 5 randomly selected fields at ×100 magnification. The data presented as the mean ± SEM (n=5 per each group of mice). (D, E) Impaired functional performance. Serum levels of albumin (D) and aspartate aminotrasferase (E) presented as the mean ± SEM (n=3 per group/per time point). (F) Reduced expression of c-Met downstream targets. Representative western blots and densitometry of phosphorylated protein levels relative to β-actin used as internal control. Data represent means ± SEM of 3 experiments. *, $P < 0.05$; **, $P < 0.01$; ***, $P < 0.001$. NT, no treatment.

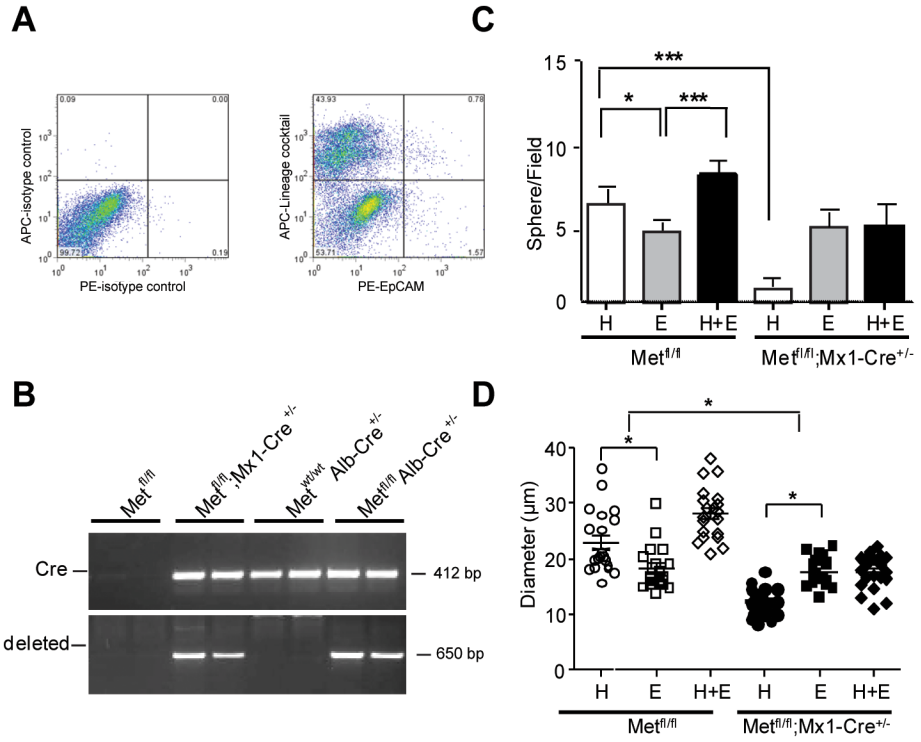

Fig.2.

Reduced sphere-forming activity of c-Met deficient oval cells. (A) FACS analysis using PE-EpCam and APC-Lineage cocktail antibodies. Representative FACS plots of isotype controls and double staining are shown. PE-EpCam^{+}/APC-Lineage^{-} cells were FACS sorted from the bulk nonparenchymal cells isolated at 2 weeks of DDC diet (n=3). The lines separate the negative and the positive cell populations, and the numbers indicate the percentages of cell counts to total population in each quadrant. (B) PCR analysis of genomic DNA. Ten thousand of EpCam^{+}/Lineage^{-} oval cells were FACS sorted from Met$^{fl/fl}$; Met$^{fl/fl}$;Mx1-Cre$^{+/-}$, c-Met$^{fl/fl}$; Alb-Cre$^{+/-}$ and c-Met$^{wt/wt}$; Alb-Cre$^{+/-}$Cells mice directly to DNA lysis buffer and subjected to PCR analysisis. The frequency (C) and the size (D) of primary spheres formed by FACS-sorted EpCAM^{+}/Lineage^{-} oval cells isolated from of Met$^{fl/fl}$;Mx1-Cre$^{+/-}$ mice. Cells were mixed with matrigel (1:1) and cultured in non-adherent condition in the presence of HGF (H, 50 ng/ml), EGF (E, 20 ng/ml), or both growth factors (H+E) for 2 weeks. Growth factors were changed every two days. Spheres were counted in 10-randomly selected fields from each sample at ×400 magnification, and the diameter of 20-randomly selected spheres was measured using NIH ImageJ 1.30 (NIH, Bethesda, MD). Results are shown as means ± SEM. *, $P < 0.05$; ***, $P < 0.001$.

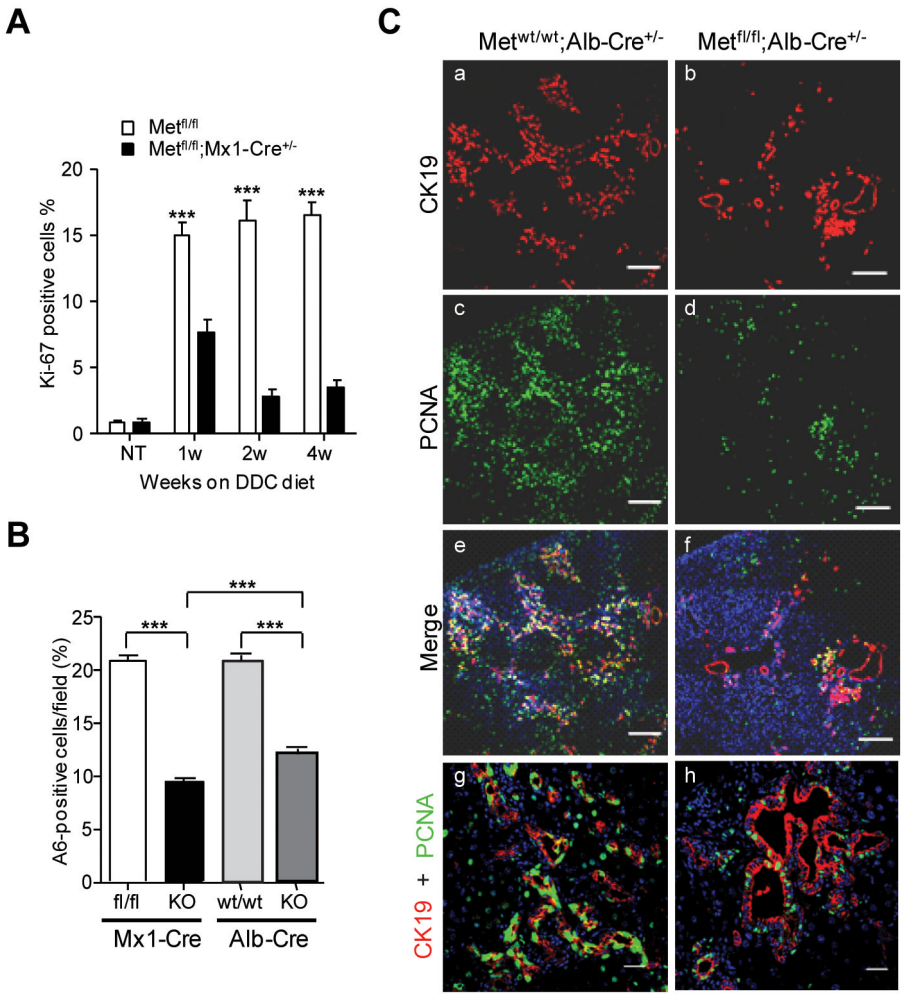

Fig. 3.

Decreased size of oval cell pool. (A) Effect of *c-met* deletion on rate of oval cell proliferation was evaluated by Ki-67 immunostaining. Cell counting was performed on 5 independent fields randomly selected at ×200 magnification at 0, 1, 2, and 4 weeks after DDC treatment. The data are presented as mean ± SEM (n=3). (B) The percent of $A6^+$ cells at 4 weeks after DDC treatment was determined in 5 independent images of portal areas taken with confocal microscope at ×200. Nuclei were counterstained with DAPI. Data are presented as mean ± SEM (n=3). ***, $P < 0.001$. (C) Double immunufluorescence staining with CK19 and PCNA shows a significant decrease in proliferation of c-$Met^{fl/fl}$; Alb-$Cre^{+/-}$ oval cells as compared to the corresponding control $Met^{wt/wt}$;Alb-$Cre^{+/-}$ oval cells. Nuclei were counterstained with DAPI. The image taken with Zeiss 570 NLO confocal microscope consist of 3×3 tiling to give total 2124.10 μM × 2124.10 μM. Scale bars, 250 μM. Representative images at higher magnification are shown at the bottom (scale bars 25 μM).

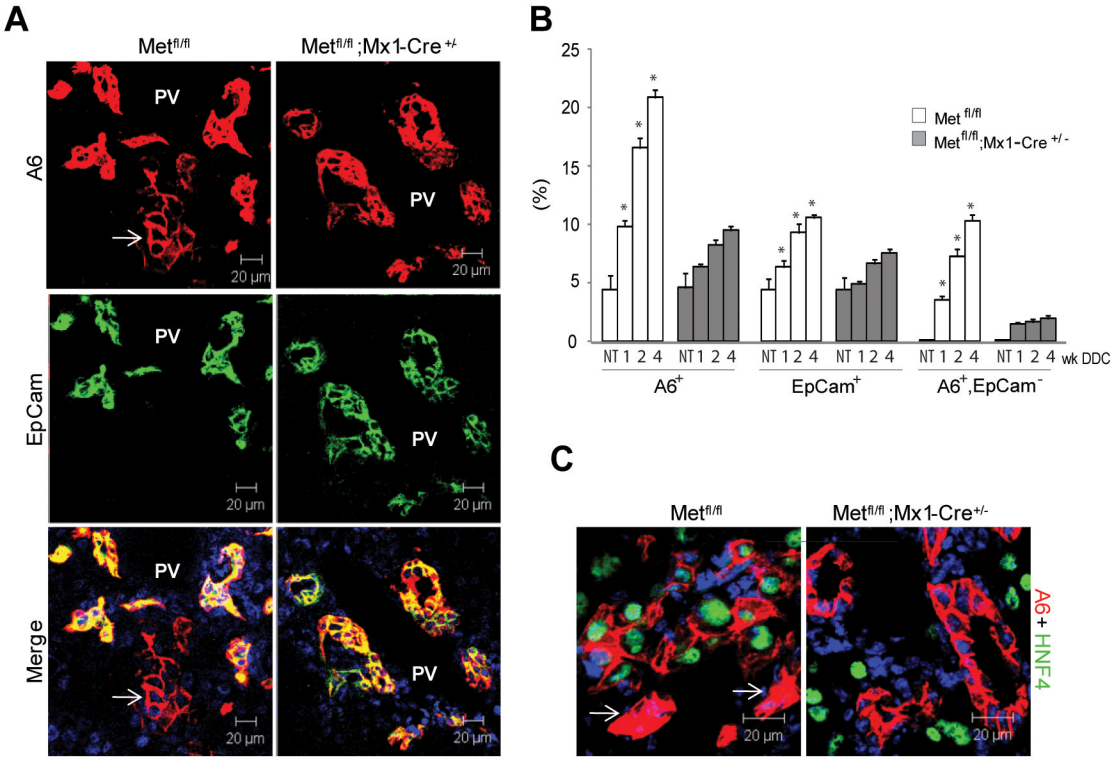

Fig. 4.

Impaired differentiation of oval cells to hepatocytes. (A) Double immunofluorescence for A6, a marker of oval cells, biliary epithelial cells and newly formed hepatocytes[33-34] and EpCam, a marker of oval cells and biliary epithelial cells[32, 35]. Representative images show the presence of $A6^+/EpCam^-$ hepatocyte-like cells (white arrow) located in the close proximity to double positive $A6^+/EpCam^+$ oval cells only in control $Met^{fl/fl}$ livers. Nuclei were counterstained with DAPI. PV, portal vein; scale bars, 20 μM. (B) Quantification of $A6^+$, $EpCam^+$, and $A6^+/EpCam^-$ cells at 1, 2 and 4 weeks after DDC treatment. The areas occupied by $A6^+$, $EpCam^+$, and $A6^+/EpCam^-$ cells were determined in 5 independent images taken with confocal microscope at ×200 and expressed as percent. Data represent mean ± SEM (n=3 mice). *, $P < 0.001$ as compared to respective cells in c-$Met^{fl/fl}$; Mx1-$Cre^{+/-}$ mice. NT, no treatment. (C) Expression of hepatocyte-specific transcription factor HNF4α in A6-positive hepatocyte-like cells which appear larger than the neighboring single A6-positive oval cells (white arrow). Nuclei were counterstained with DAPI. Scale bars, 20 μM.

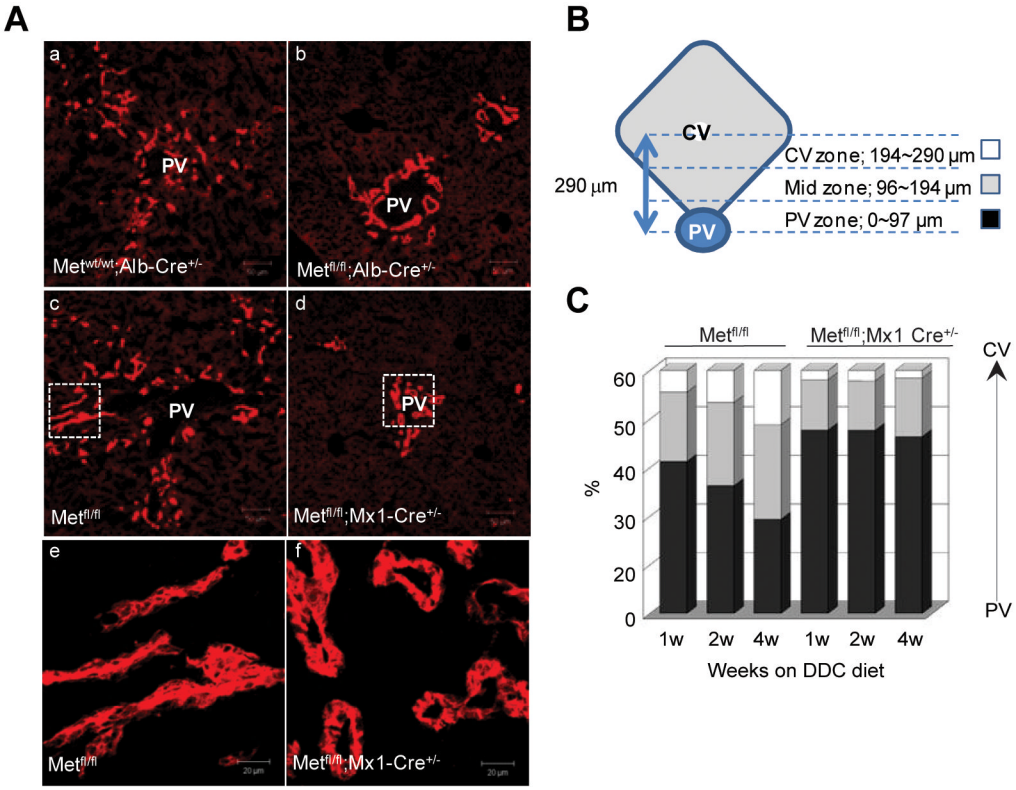

Fig. 5.

Lobular distribution and staining pattern of ductular reaction. (A) Representative photos of oval ductular cells at 4 weeks of DDC treatment visualized by A6 immunoflourescence. Scale bar, 50 μm. Enlarged images of the boxed areas from the middle panels are shown in the bottom. Scale bar, 20 μm (B, C) Hepatic lobule was divided into three zones, including periportal (PV, 0-97 μm), middle (97-194 μm), and central (CV, 194-290 μm), and the percentage of $A6^+$ cells in each zone was determined at each time point using 5 independent images taken with confocal microscope at ×400. Data represent mean ± SEM (n=3 mice per genotype at each time point). The frequency of $A6^+$ cells reaching middle and central zones were progressively increasing only in control $Met^{fl/fl}$ mice.

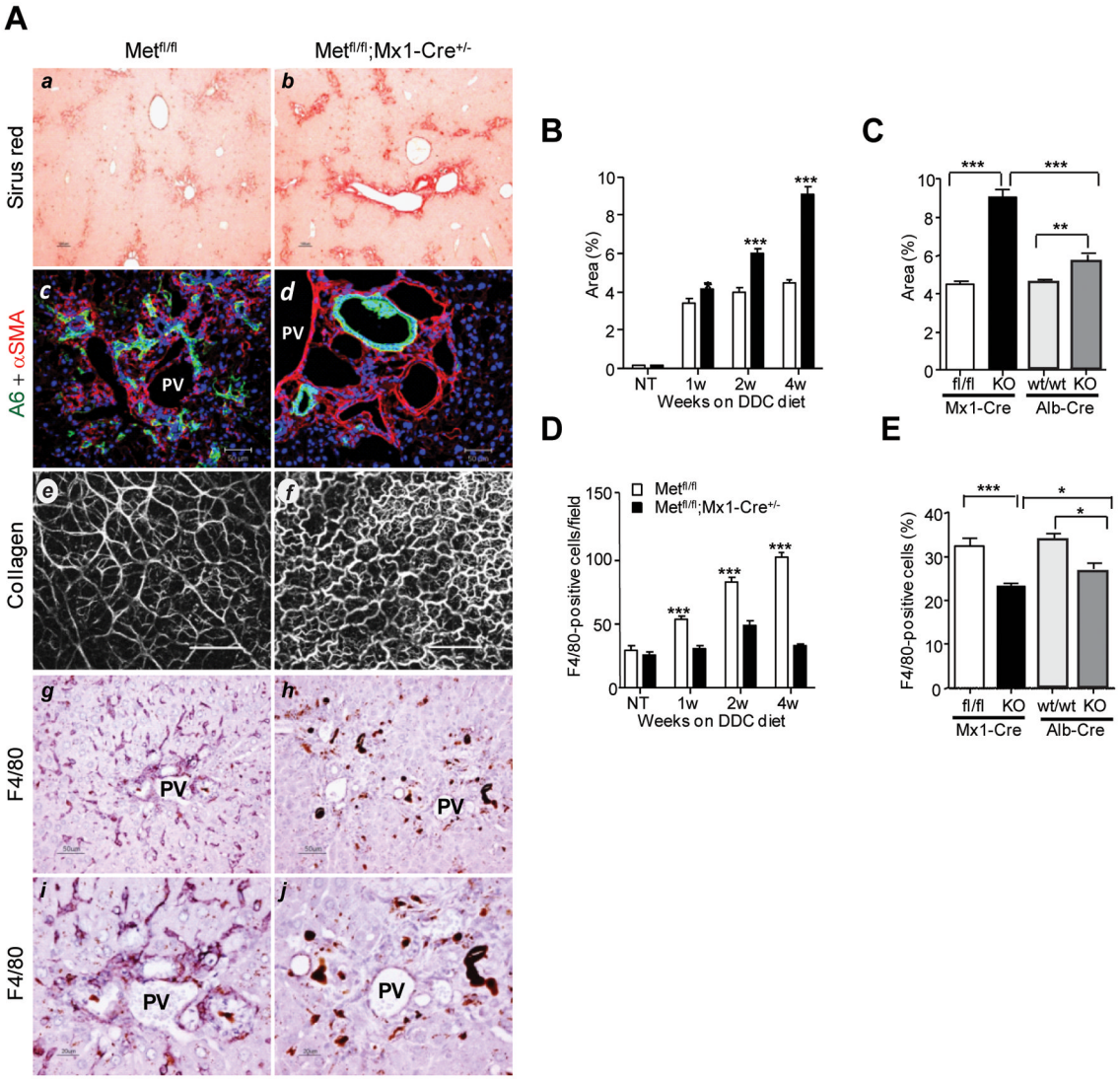

Fig. 6.

Defective tissue remodeling during hepatic progenitor cell response in c-Met deficient livers. (A) Representative photos of Sirius red staining (*a*,*b*), A6 and αSMA double fluorescence staining (*c*,*d*), Second-harmonic generation images of collagen fibers in unfixed livers (*e*,*f*), and F4/80 immunohistochemical staining (*g*-*j*). Images were taken with light microscopy at 4 weeks (*a*-*d* and *g*-*j*) and with confocal microscopy (LSM 710 NLO) at 2 weeks (*e*,*f*) after initiation of DDC diet. Scale bars, 100 μm (*a*,*b*); 50 μm (*c*-*d* and *g*-*h*); 200 μm (*e*,*f*), and 20 μm (*i*,*j*). PV, portal vein. (B) Hepatic fibrosis was assessed by morphometric analysis of Sirius red staining carried out on 5 images taken with light microscopy using NIH ImageJ 1.30. Fibrotic area was calculated as [Sirus red stained area/(total area – vascular lumen area)×100 %. Data represent mean ± SEM (n=3 mice). (C) The graph displays percent of Sirus-red areas in livers with total ($Met^{fl/fl}$;$Mx1\text{-}Cre^{+/-}$) and selective ($Met^{fl/fl}$;$Alb\text{-}Cre^{+/-}$) c-Met deletion at 4 weeks of DDC diet. Data represent mean ± SEM (n=3). (D) The kinetic changes in the frequency of $F4/80^+$ cells. The number of $F4/80^+$ Kupffer cells was determined at 1, 2, and 4 weeks after DDC treatment using 5 independent images taken with light microscopy at ×200 magnification. Data represent mean ± SEM (n=6). (E) Reduced frequency of $F4/80^+$ Kupffer cells in livers with total ($Met^{fl/fl}$;Mx1-

$Cre^{+/-}$, n=6) and selective ($Met^{fl/fl}$;Alb-$Cre^{+/-}$, n=3) c-Met inactivation. The bulk nonparenchymal cells were isolated at 2 weeks after DDC treatment and subjected to FACS analysis using anti-F4/80. 50,000 events were collected. Data represent mean ± SEM (n=3). *, $P < 0.05$; **, $P < 0.01$***, $P < 0.001$.

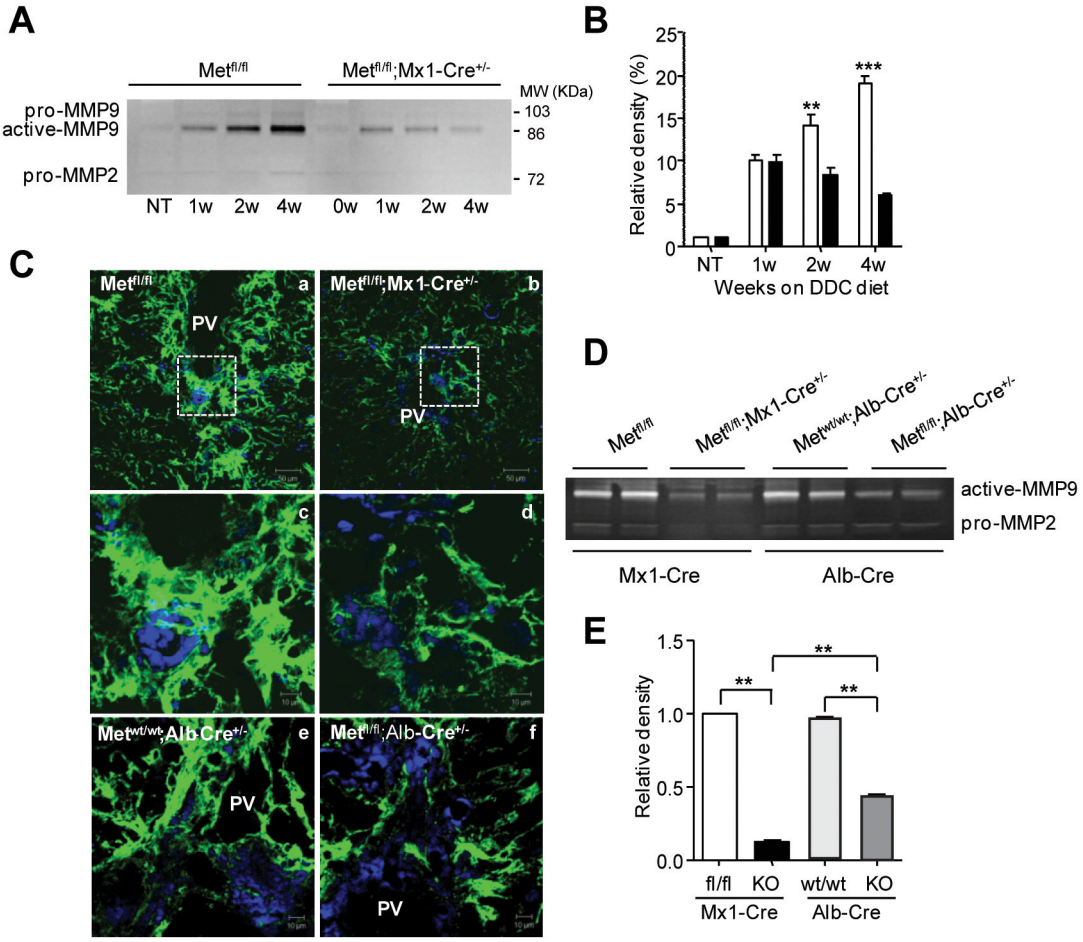

Fig. 7.

Reduced MMP9 activity during hepatic progenitor cell response in c-Met deficient mice. (A) Gelatinolytic activity in liver tissue determined by zymography. Representative inverted black-and-white images of gelatin zymography are shown. Enzymatic activity was inhibited in the presence of an MMP inhibitor (10 mM EDTA) (not shown). (B) Quantification of MMP9 activity by densitometry. Data represent mean ± SEM of three independent experiments expressed as percent versus values in untreated $Met^{fl/fl}$ mice. (C) Representative images of in situ zymography performed at 4 weeks after DDC treatment on frozen liver sections from mice with total ($Met^{fl/fl}$;Mx1-$Cre^{+/-}$) and selective ($Met^{fl/fl}$;Alb-$Cre^{+/-}$) *c-met* deletion and their respective controls ($Met^{fl/fl}$) and ($Met^{wt/wt}$;Alb-$Cre^{+/-}$) taken with confocal microscopy. Protease activity is observed as a strong green fluorescence signal against a dark background. Enlarged images of the boxed areas from the top shown in the middle demonstrate a predominant accumulation of MMP9 activity in the periportal areas. PV, portal vein. Scale bars, 50 μM (top); 10 μM. (D and E) Representative gelatin zymography and quantification of MMP9 activity in livers with total ($Met^{fl/fl}$;Mx1-$Cre^{+/-}$) and selective ($Met^{fl/fl}$;Alb-$Cre^{+/-}$) *c-met* deletion at 4 weeks of DDC diet relative. Data represent mean ± SEM of three independent experiments expressed as a relative density versus values in Met $^{fl/fl}$ mice. **, $P < 0.01$***, $P < 0.001$.

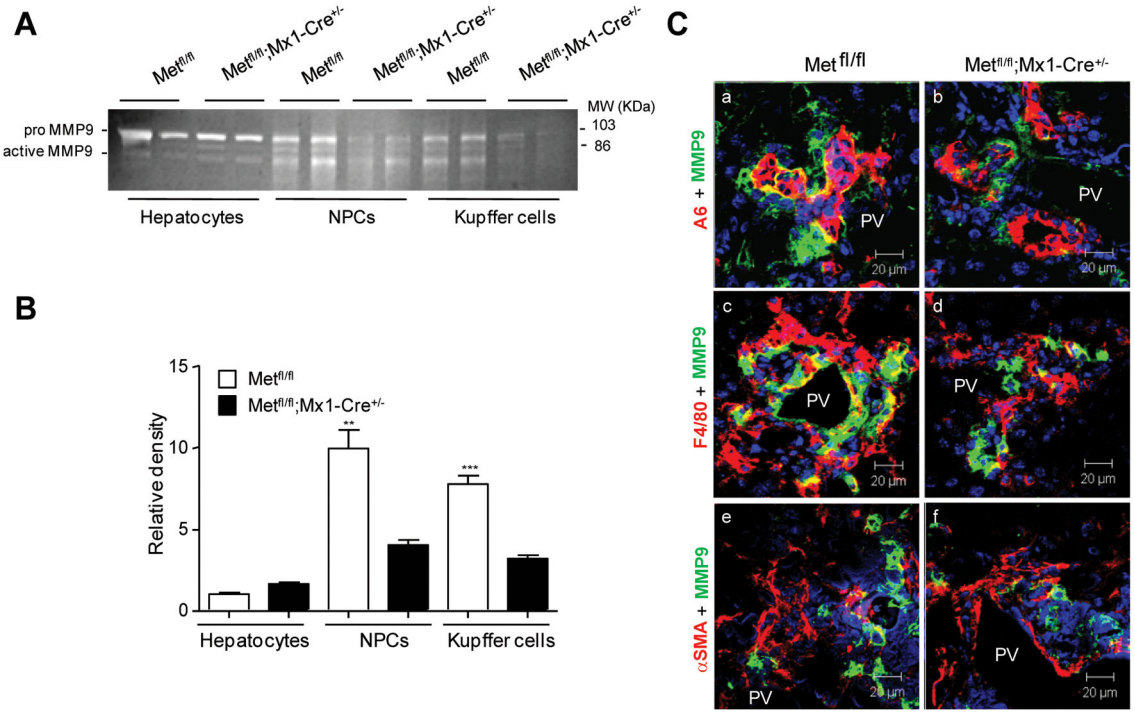

Fig. 8.

Cell source of MMP9 in DDC model of liver injury. (A) Gelatinolytic activity in isolated hepatocytes, nonparenchymal cells and FACS-sorted F4/80^{+} monocytes/macrophages at 2 weeks after DDC treatment. Representative inverted black-and-white images of gelatin zymography are shown. (B) Quantification of MMP9 activity by densitometry. Data represent mean ± SEM of three independent experiments expressed as a relative density versus values in Met $^{fl/fl}$ hepatocytes. **, $P < 0.01$***, $P < 0.001$. (C) Representative images of double immunofluorescence of MMP9 (green) with A6 (top); F4/80 (middle) and αSMA (bottom) at 4 weeks after DDC treatment. PV, portal vein. Scale bars, 20 μM.